AGU PUBLICATIONS

Radio Science

RESEARCH ARTICLE
10.1002/2013RS005203

Digital transmission techniques for a long haul HF link: DSSS versus OFDM

P. Bergadà[1], R. M. Alsina-Pagès[1], J. L. Pijoan[1], M. Salvador[1], J. R. Regué[1], D. Badia[1], and S. Graells[1]

[1]GRECO-La Salle, Universitat Ramon Llull, Barcelona, Spain

Key Points:
- Advanced modulation techniques applied to HF communications
- Spread spectrum and OFDM modulations for ionospheric transmissions

Correspondence to:
R. M. Alsina-Pagès,
ralsina@salleurl.edu

Citation:
Bergadà, P., R. M. Alsina-Pagès, J. L. Pijoan, M. Salvador, J. R. Regué, D. Badia, and S. Graells (2014), Digital transmission techniques for a long haul HF Link: DSSS versus OFDM, *Radio Sci.*, *49*, 518–530, doi:10.1002/2013RS005203.

Received 22 NOV 2013
Accepted 26 JUN 2014
Accepted article online 30 JUN 2014
Published online 21 JUL 2014

Abstract This paper presents two digital transmission techniques for long haul ionospheric links. Since 2003 we have studied the HF link between the Antarctic Spanish Base, Juan Carlos I, and Spain; and we have described the link in terms of availability, signal-to-noise ratio, and delay and Doppler power profile. Based on these previous studies we have developed a test bed to investigate two digital transmission techniques, i.e., Direct-Sequence Spread Spectrum (DSSS) and Orthogonal Frequency Division Multiplexing (OFDM), which can provide a low power, low-rate ionospheric data link from Antarctica. Symbol length, bandwidth, and constellation are some of the features that are analyzed in this work. Data gathered from the link throughout the 2010/2011 and 2011/2012 Antarctic surveys show that the spread spectrum techniques can be used to transmit data at low rate when the channel forecast is poor, but when the channel forecast is good multicarrier techniques can be used to transmit sporadic bursts of data at higher rate.

1. Introduction

Much has been achieved during the last two decades to improve the spectral efficiency of new mobile communication services. Although there are many differences between the UHF and HF bands, sky wave narrowband HF propagation can be modeled as a slow fading multipath channel [*Gherm et al.*, 2005]. Multiple paths arise from the refraction of HF waves in the different layers of the ionosphere and from multihop propagation. Moreover, within each path the wave splits into two modes, which are called ordinary (O) and extraordinary (X). These two phenomena cause frequency selectivity and degrade the signal to noise ratio, which can be combated with wideband signals plus coding and interleaving.

Many of the modulation and coding techniques applied to third and fourth generation mobile communications can be adapted to the HF band. Frequency Hopping (FH) [*Andersson*, 1994] and Direct Sequence (DS) [*Wagner et al.*, 1989] were the first spread spectrum (SS) modulations proposed for the HF band. FHSS and DSSS are intrinsically designed to perform well against narrowband interference and to benefit from frequency diversity in frequency selective channels, which are key issues in the HF channel. Therefore, they have been adopted in the robust mode of several NATO standards [*NATO*, 1999].

Orthogonal Frequency Division Multiplexing (OFDM) is another successful technique that uses multicarrier transmission to overcome the problems of multipath channels. This includes new constant envelope OFDM modulation schemes, e.g., Single Carrier OFDM [*Myung and Goodman*, 2008] and Constant Envelope OFDM [*Nieto*, 2008], which are well adapted to HF channels.

Military research uses OFDM as a communication technique in the HF channel. MIL-STD-188-110A [*US Department of Defense*, 1991] describes a single tone and two multitone (16-tone and 39-tone) OFDM-based modem with a maximum bit rate of 2400 bps. In later improvements, *Gill et al.* [1995] applied trellis-coded modulation to create redundant bits for error control purposes. The use of convolutional trellis codes combined with interleaving resulted in a 300 to 3600 bps modem that provided immunity to impulsive noise and narrowband interference.

High-data rate HF systems typically need signal-to-noise ratios (SNR) greater than 20 dB to properly work in a 3–25 kHz channel. With a 25 dB SNR, bit rates up to 16 kbps for a bit error rate (BER) = 10^{-2} can be achieved [*Zhang et al.*, 2005]. Bandwidths up to 24 kHz have been standardized, and bit rates up to 120 bps may be achieved in optimum conditions [*Furman and Nieto*, 2012; *Johnson*, 2009], and greater bandwidths out of standardization are also being tested [*D'Orazio et al.*, 2007]. Moreover, the use of several noncontiguous 3 kHz channels has also been investigated [*Smith et al.*, 2001]. In contrast, NATO has standardized a serial-tone modem (STANAG 4415) for severely degraded HF radio links which is able to work at negative SNR

in a 3 kHz bandwidth [*NATO*, 1999]. The penalty is a low-bit rate. STANAG 4415 uses Walsh codes of length 32 achieving 75 bps in a 3 kHz bandwidth. It uses a 4.8 s interleaver combined with a rate $\frac{1}{2}$ convolutional encoder [*NATO*, 1999].

It is well known that HF communication is a good option for very long radio links where no other infrastructure (e.g., satellite) is available. In that regard, our research group has been investigating the HF channel (herein referred to the Antarctic channel) between the Spanish Antarctic Station (SAS) on Livingston Island (62.6°S, 60.4°W) and the Ebro Observatory (EO) in Roquetes (40.8°N, 0.5°E), Spain. We have sounded this channel throughout a whole solar cycle to characterize the availability, SNR, multipath, and Doppler power profile [*Vilella et al.*, 2008]; we have linked vertical soundings along the path with oblique soundings [*Vilella et al.*, 2009]; and we have developed a low power, adaptive communication system for data transmission from remote sensors.

Ours is a very long transmission path (12,700 km, 4–5 hops [*Perkiomaki*, 2013]), which together with a transmitter power of only 200 W and very simple antennas at the transmission and reception sites, due to environmental restrictions. This results in very low or even negative SNR at the receiver [*Vilella et al.*, 2008].

Even the robust mode of STANAG 4415 would have problems to work in this scenario. STANAG 4415 is designed to work in severe scenarios of Doppler spread (i.e., up to 20 Hz) and delay spread (i.e., up to 10 ms) achieving a BER $< 10^{-4}$. However, STANAG 4415 requires SNRs above −1 dB to 0 dB (3 kHz) in a dual path channel. The Antarctic channel SNR is typically lower than −6 dB, with Doppler spreads up to 2 Hz, and the maximum delay spread is 3 ms [*Ads et al.*, 2012]. Consequently, we have concluded that STANAG 4415 is not well matched to the Antarctic channel. To mitigate the channel STANAG 4415 would need to be modified and use longer symbols (or equivalently narrower frequency symbols) in order to cope with such a low SNR; however, then it would not perform well in fast fading channels.

Consequently, we have designed a physical layer adapted to low SNR, time and frequency dispersive channels, and high interference occurrence, based on both DSSS [*Deumal et al.*, 2006] and OFDM [*Bergadà et al.*, 2009] techniques. Due to the distance, the low-transmitted power, and antenna constraints, the received SNR is low. As a result, the transmitted bandwidth must be very narrow and only low-bit rates can be achieved; hence, the spectral efficiency is the key. The challenge is to increase the efficiency of the link in the available bandwidth.

In this study we explore the use of DSSS and OFDM techniques for very long and power limited HF links, using various bandwidths and bit rates, taking into account the outcomes and impairments described in *Vilella et al.* [2008] and *Ads et al.* [2012].

2. Link and System Description

One of the main objectives of our work is to establish a permanent HF link between the SAS and the EO. The propagation conditions between both sites vary daily, seasonally, and with the solar cycle. The first oblique sounding of the Antarctic channel was performed during the 2003/2004 survey, and since then, three software defined radio hardware system upgrades have been installed at both the transmitter and the receiver sides.

The last generation platform was installed in the 2009/2010 survey, and all the results in this paper are based on this upgrade. The system is currently able to operate over the full HF band (from 3 MHz to 30 MHz), 24 h a day.

The system combines both channel sounding periods and data transmission periods. Each hour the whole HF band is sounded in narrowband and wideband modes for 40 min, and data are transmitted for 10 min, see *Ads et al.* [2012] for a more detailed explanation of the system and the sounding process.

3. Test Design

In the design of an HF radio modem able to work on very long links with low-transmission power, several important issues need to be considered. First, the selection of the best carrier frequency must consider the whole path and satisfy the constraints of the most restrictive hop. Second, once the transmission power and the antenna are selected, the maximum bandwidth will be fixed by the required SNR at the receiver. If this bandwidth is higher than the coherence bandwidth of the channel (i.e., 150–500 Hz in our case

Table 1. Detail of the PN Sequence Length, Bandwidth, Corresponding Bit Rate, Symbol Time, and Spectral Efficiency[a]

PN Sequence Length	BW (kHz)	T (ms)	Bit Rate (bps)	Spectral Efficiency (bps/Hz)	CDF (10%)	CDF (30%)	CDF (50%)	CDF (70%)
31	20	1.5	645.16	0.032	0.2910	0.3330	0.3330	0.3740
31	10	3.1	322.58	0.032	0.2490	0.3330	0.3740	0.3740
31	5	6.2	161.29	0.032	0.2910	0.3330	0.3740	0.3740
31	2	15.5	64.52	0.032	0	0.0830	0.2490	0.3330
31	1	31.0	32.26	0.032	0	0	0.1240	0.2490
31	0.50	62.0	16.13	0.032	0	0	0.1240	0.2490
31	0.25	124.0	8.06	0.032	0	0	0.0830	0.2490
63	20	3.1	317.46	0.016	0.2910	0.3740	0.3740	0.3740
63	10	6.3	158.73	0.016	0.2910	0.3330	0.3740	0.3740
63	5	12.0	79.36	0.016	0	0.1660	0.2910	0.3330
63	2	31.0	31.75	0.016	0	0.0410	0.0830	0.2080
63	1	63.0	15.87	0.016	0	0.0410	0.1240	0.2910
63	0.50	126.0	7.94	0.016	0	0	0.1240	0.2490
63	0.25	252.0	3.97	0.016	0	0.1240	0.2490	0.3330
127	20	6.3	157.48	0.007	0.2910	0.3330	0.3330	0.3740
127	10	12.7	78.74	0.007	0.1660	0.2910	0.3330	0.3740
127	5	25.4	39.37	0.007	0	0.1240	0.2910	0.3330
127	2	63.0	15.75	0.007	0	0.0410	0.1660	0.2910
127	1	127.0	7.87	0.007	0	0.0830	0.2080	0.2910
127	0.50	254.0	3.94	0.007	0	0.1660	0.2490	0.2910
127	0.25	507.0	1.97	0.007	0.1240	0.2490	0.3330	0.3740

[a]The spectral efficiency is always the inverse proportion of the PN sequence length when a constant sampling frequency is used, and the bit rate is the inverse of the symbol time since Differential Binary Phase Shift Keying (DBPSK) is used. The values of cumulative distribution function of the BER are given for all the designed combinations. CDF, cumulative distribution function.

[*Ads et al.*, 2012]), the use of wideband modulations that are robust against frequency selective channels may be considered. DSSS and OFDM are the most well-known schemes for slow fading, multipath channels such as the ionospheric channel [*Proakis*, 2000].

In this paper we compare the behavior of different transmission schemes based on DSSS and OFDM techniques, and we present some conclusions that derive from the data gathered during the 2010/2011 and 2011/2012 Antarctic surveys. Previous results [*Bergadà et al.*, 2009] showed preliminary conclusions supported on a reduced frequency and time range.

3.1. Direct-Sequence Spread Spectrum

In this section we explore DSSS [*Proakis*, 2000; *Peterson et al.*, 1995] as a possible solution to the frequency selectivity of the Antarctic channel.

When using DSSS techniques, the signal is spread over a wide bandwidth, proportional to a pseudo noise (PN) chip rate, which provides robustness against narrowband interfering signals. A drawback of DSSS is the low-spectral efficiency symbols that may need to achieve good bit error rate (BER) performance. Its main advantage is that no channel estimation is needed.

We transmitted DSSS signals with different symbol lengths and bandwidths by changing the chip rate and the PN sequence length in order to determine which of the DSSS parameters best match the Antarctic channel. We have determined the maximum bit rate with an acceptable BER, assuming that no channel coding is used. Given that the channel is time varying, we have also determined the upper bound of the symbol period, this being limited by the coherence time of the channel.

3.1.1. DSSS Symbol Design

DSSS spreads a signal composed by symbols of length T by means of a PN sequence $c(t)$. The PN sequence is formed by L chips of length T_c with good autocorrelation and cross-correlation properties, such that $L \cdot T_c = T$. L is known as the spreading factor and is the ratio between the spread bandwidth and the original signal bandwidth.

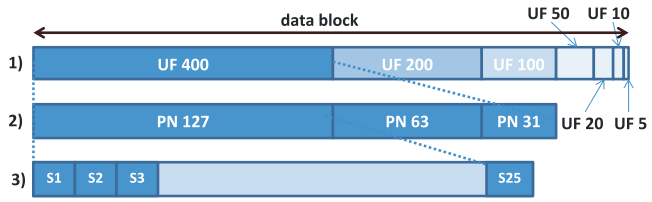

Figure 1. Graphic detail of the DSSS data block design. (row 1) The order depending on the bandwidth, which is a function of the number of samples per chip or Up Factor (UF). (row 2) The symbols are sorted considering the PN sequence length. (row 3) The detail of the 25 symbols used for each of the previously described combinations.

3.1.2. DSSS Test Details

The DSSS tests were conducted using various bandwidths, bit rates, sequence lengths, and samples per xip (at fixed sample rate, i.e., 100 kHz). These four variables were modified according to previous knowledge of the channel [*Ads et al.*, 2012]: (1) Bandwidth (BW): from 250 Hz to 20 kHz, (2) Bit rate: from 1.97 bps to 645 bps, (3) PN sequence length: 31, 63, and 127 chips, (4) Samples per chip: 5, 10, 20, 50, 100, 200, and 400.

We used Gold spreading sequences [*Gold*, 1968] with length $2^n - 1$, and we chose a minimum sequence length of 31, because shorter sequences could not be detected in such a noisy scenario. Table 1 details DSSS tests, including bandwidth, symbol length T, bit rate, and spectral efficiency. The outcomes are based on average of 148 blocks of data. Each block of data is composed of 21 experiments (see Table 1), and for each experiment 25 DSSS symbols were transmitted. Figure 1 describes the data block design.

Previous work on this channel [*Ads et al.*, 2012] showed that the coherence time of the Antarctic channel ranges from 500 ms to 1 s depending on the time of day, so some of the combinations enumerated in Table 1 (i.e., 400 samples per chip and 127 chips per sequence) go beyond the coherence time and hence should show worse performance than other combinations with shorter T. Conversely, those codes with low samples per chip and a short sequence length (i.e., 5 samples per chip and 31 chips per sequence) exhibit a low probability of detection and hence a poor performance. Between these two points we should be able to show optimum combination of bandwidth and PN sequence length.

We note that none of the combinations provide a data throughput sufficient to support real-time voice or image transmission, but all are sufficient for our application [*Bergadà et al.*, 2009].

3.1.3. Timing Synchronization and Channel Estimation

Timing synchronization is a critical task in a DSSS receiver [*Proakis*, 2000]. The DSSS modulation described in this paper does not use any preamble but uses a number of sequences for synchronization purposes. The longest tests (i.e., PN sequence length of 127 chips and 400 samples per chip) are located at the beginning of the data stream, and fine time synchronization is performed by means of correlation [*Proakis*, 2000] over these symbols. The acquisition point is expanded to later PN sequences with higher bandwidth and shorter length of the same block. Tracking the channel performance and correcting the acquisition point are implemented when necessary while analyzing the data block.

The channel estimation and the demodulation process is performed by correlating the received signal by a delayed copy of the transmitted sequences, which is the best acquisition method in terms of BER outcomes [*Proakis*, 2000]. The downside of this method is the high computational cost at the receiver.

3.2. Orthogonal Frequency Division Multiplexing

We also explored OFDM because its spectral efficiency is higher than DSSS. The OFDM symbol must be adapted to the specific channel and its drawbacks of intercarrier interference (ICI) and peak to average power ratio (PAPR) must be carefully examined.

Our OFDM study transmitted symbols with different characteristics (i.e., time length, bandwidth, constellation, and input back-off) over the 5 hop HF channel to find which OFDM design characteristics best fit the channel. In a frequency selective channel in our case with a coherence bandwidth $BW_c \in$ (150 Hz, 500 Hz) [*Ads et al.*, 2012] the OFDM bandwidth has to be wider than the BW_c to benefit from frequency diversity. However, this cannot be arbitrarily bigger because the larger the number of subcarriers the lower the SNR per subcarrier. Furthermore, intercarrier space cannot be arbitrarily wide because it must fulfill the Nyquist criterion to enable the equalizer to rebuild the channel. Moreover, the OFDM symbols also face a time variant channel (with coherence time $T_c \in$ (500 ms , 1 s) [*Vilella et al.*, 2008]); and hence, when seeking high efficient symbols the length cannot be arbitrarily long, otherwise it may exceed the coherence time of the channel. Finally, the issue of saturation of the transmitter power amplifier has to be considered. This

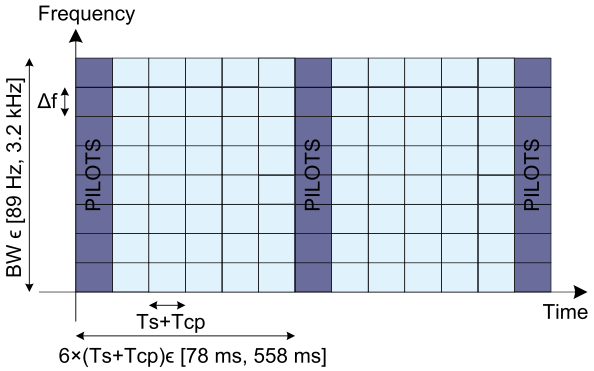

Figure 2. OFDM pilots lattice for channel estimation and equalization.

problem arises from the coherent addition of the OFDM signal components and is commonly dealt with reducing the drive to the transmitter.

3.2.1. OFDM Symbol Design

Orthogonal multicarrier modulation divides a single stream of symbols with length T into N_c streams with longer length N_cT. Let us define the OFDM symbol in the time domain, $x(t)$, as

$$x(t) = \frac{1}{\sqrt{N_c}} \sum_{k=0}^{N_c-1} X_k e^{j2\pi f_k t},\ -T_{\text{cp}} < t < N_cT, \tag{1}$$

where X_k are the frequency domain symbols that we allocate on each of the N_c subcarriers. The subcarriers are equally spaced $f_k = \frac{1}{N_cT}$ Hz, which make them orthogonal. If we cyclically repeat $N_{\text{cp}} = T_{\text{cp}} \times f_{\text{sampling}}$ samples, [*Peled and Ruiz*, 1980], at the beginning of each OFDM symbol, it preserves orthogonality and immunity to time dispersive channels whenever T_{cp}, which is the cyclic prefix guard time, exceeds the channel impulse response (τ_c). *Ads et al.* [2012] concluded that τ_c varies in time and frequency but it is always shorter than 3 ms in the Antarctic channel; hence, the length of the cyclic prefix in all the multicarrier transmissions is fixed to 3 ms. The cyclic prefix appended to the start of each OFDM symbol reduces the spectral efficiency $\left(\rho_1 = \frac{N_cT}{N_cT+T_{cp}}\right)$ of the system; however, a time symbol much longer than the cyclic prefix minimizes this drawback.

3.2.2. Frequency and Timing Synchronization

We have used two oven controlled crystal oscillators with high stability features (±0.1 ppb/°C and ±30 ppb versus aging per year), as well as ultralow jitter and phase noise features ($-125\ \text{dBc/Hz}|_{10\ \text{Hz}}$ at 10 MHz). Consequently, no frequency synchronization techniques were necessary and no ICI effects were present, so only timing synchronization has been implemented. Due to the low SNR expected at the receiver, neither a technique based on pilot insertion in OFDM symbols [*Moose*, 1994; *Schmidl and Cox*, 1997] nor a technique that exploits intrinsic redundancy based on the repetition of the N_{cp} samples of the cyclic prefix [*Tourtier et al.*, 1993; *Sandell et al.*, 1995] is expected to work. Therefore, we designed a preamble composed of 40 maximal length pseudo noise sequences [*Golomb*, 1967], with good autocorrelation properties, 256 chips each and a bandwidth of 10 kHz. This preamble performs time acquisition at the beginning of the stream and time tracking every 12 s on average. It can also be used to estimate the channel impulse response, hence its wide bandwidth.

Clock deviation between transmitter and receiver causes a cumulative windowing position offset. However, the accumulated timing offset due to the tolerance of the clocks (±0.1 ppb) can be neglected because we transmit long symbols, with low number of subcarriers, and low complexity constellations.

3.2.3. Channel Estimation

In this OFDM study we coherently encoded the symbols of each subcarrier by means of a phase shift keying modulation, although we could design a simpler and even a more efficient receiver without the pilot symbol overhead, as proposed by *Engels and Rohling* [1995] for Digital Audio Broadcasting. In extreme low SNR scenarios, coherent modulation outperforms differential modulation since coherent decoding process includes channel state information [*Baum et al.*, 1997].

We defined a pilot pattern (see Figure 2) to perform the channel estimation by means of the least squares algorithm and 2-D cubic splines interpolation.

The pilot grid of the channel estimator must fulfill the two dimensional sampling theorem [*Hoeher et al.*, 1997] to properly track channel time and frequency variability. This means that pilot separation in frequency is upper bounded by

$$N_F \leq \left\lfloor \frac{\text{BW}_c}{2\Delta f} \right\rfloor \tag{2}$$

and in time by

$$N_T \leq \left\lfloor \frac{T_c}{2N_c T} \right\rfloor. \tag{3}$$

However, if we choose N_T and N_F close to 1 the efficiency of the system decreases and consequently decreases the SNR, as well as the throughput of the link. So there is a trade-off between efficiency and performance that, taking into account previous studies on this channel [*Vilella et al.*, 2008; *Ads et al.*, 2012], we have resolved as (i) $N_F = 1$ since the lower bound of the coherence bandwidth of the channel (150 Hz) is similar to the subcarrier separation tested in this study $\{11.0, 14.2, 20.0, 33.0, 100.0\}$ (Hz), and (ii) $N_T = 6$ since the lower bound of the coherence time of the channel (500 ms) is much higher than the length of the OFDM symbols, $\{10, 30, 50, 70, 90\}$ (ms). Consequently, the efficiency (ρ_2) and the loss of SNR ($1 - \rho_2$) can be computed as

$$\rho_2 = \frac{N_T \cdot N_F - 1}{N_T \cdot N_F}\Big|_{N_F=1, N_T=6} = 83.3\%, \tag{4}$$

and the final efficiency of the system for each OFDM symbol length transmitted in this study (see Table 2) is then

$$\rho = \rho_2 \cdot \rho_1 \in [64.0,\ 80.6]\%. \tag{5}$$

Figure 2 depicts the pilot grid.

3.2.4. Peak to Average Power Ratio

It is well known that one of the most important drawbacks of multicarrier systems is the PAPR. The envelope variations cause the use of large back-off values in the amplifier, to avoid operating in the nonlinear region, and consequently reducing the mean transmitted power. In order to reduce the PAPR, we applied a soft limiter, which reduces the dynamic range of the signal at the expense of introducing both out-band and in-band distortion.

To reduce its effects, we limited the number of subcarriers to less than 32 (i.e., 8, 16, and 32). Moreover, the constellations that we tested are simple (Binary Phase Shift Keying (BPSK) and Quadrature Phase Shift Keying (QPSK)), which reduces the error probability introduced by the soft limiter. Finally, we oversampled each OFDM symbol to avoid aliasing by padding with zeros and taking longer inverse fast Fourier transform (IFFT) windows. We gathered 33 blocks of OFDM symbols clipped at different values of Input Back-Off (IBO), i.e., the range from the mean power of the input signal to the clipping level, and we evaluated the distortion at the receiver by means of the Error Vector Magnitude (EVM) of the constellation. On each block we transmitted 120 symbols for each IBO value (i.e., 1, 3, 5, 7, 9 , and 11 dB) with oversampling factors of 125, 250, and 500. It is worth noting that the lower the IBO the higher the in-band distortion and the higher the mean power of the transmitted signal. In a scenario with such a low SNR at the receiver side, there is a trade-off between distortion and mean transmitted power. In other words, if we reduce the PAPR by applying a soft limiter with low IBOs, we increase the in-band distortion and the mean transmitted power, whereas if we clip the signal at higher IBOs to reduce distortion, we are at the same time reducing the mean transmitted power.

4. Test Results

The conclusions that we present in this section are derive from the results gathered during the 2010/2011 and 2011/2012 Antarctic surveys. The carrier frequencies were spread across the whole HF band, and transmissions were made over a wide range of hours. The figures of merit that we use in this paper are the Error Vector Magnitude (EVM) and the Differential Error Vector Magnitude (DEVM). EVM is defined in section 4.2.1, and DEVM represents the magnitude of the error between two received signals spaced one symbol apart in time:

$$\text{DEVM}_{\text{RMS}} = \sqrt{|\text{Actual}| - |\text{Ideal}|}, \tag{6}$$

where *Actual* is the difference between two consecutive received symbols and *Ideal* is the difference between two ideal symbols. Due to the low number of received bits, these figures complement the information shown by the BER.

Table 2. Summary of the Characteristics of the OFDM Symbols Transmitted During the Tests: Symbol Length (T_s), Number of Subcarriers (N_c), BW, Modulation, IBO, Bit Rate, and Spectral Efficiency[a]

T_s (ms)	N_c	BW (Hz)	Modulation	IBO (dB)	Bit Rate (bps)	Spectral Efficiency (bps/Hz)	CDF (10%)	CDF (30%)	CDF (50%)	CDF (70%)
10	8	800	BPSK	7	512	0.641	0.14	0.31	0.38	0.44
10	16	1600	BPSK	7	1025	0.641	0.12	0.36	0.45	0.47
10	32	3200	BPSK	7	2051	0.641	0.37	0.41	0.46	0.48
10	8	800	QPSK	7	1025	1.282	0.35	0.38	0.41	0.47
10	16	1600	QPSK	7	2051	1.282	0.37	0.44	0.45	0.47
10	32	3200	QPSK	7	4102	1.282	0.43	0.45	0.46	0.50
30	8	266	BPSK	7	202	0.757	0.06	0.19	0.22	0.33
30	16	533	BPSK	7	404	0.757	0.16	0.22	0.37	0.42
30	32	1066	BPSK	7	808	0.757	0.21	0.32	0.35	0.45
30	8	266	QPSK	7	404	1.515	0.21	0.29	0.35	0.40
30	16	533	QPSK	7	808	1.515	0.47	0.48	0.49	0.50
30	32	1066	QPSK	7	1616	1.515	0.31	0.40	0.45	0.49
50	8	160	BPSK	7	125	0.786	0.08	0.11	0.14	0.26
50	16	320	BPSK	7	251	0.786	0.17	0.20	0.23	0.36
50	32	640	BPSK	7	503	0.786	0.14	0.26	0.27	0.45
50	8	160	QPSK	7	251	1.572	0.09	0.26	0.32	0.47
50	16	320	QPSK	7	503	1.572	0.25	0.31	0.37	0.47
50	32	640	QPSK	7	1006	1.572	0.28	0.44	0.48	0.50
70	8	114	BPSK	7	91	0.799	0.04	0.11	0.12	0.28
70	16	228	BPSK	7	182	0.799	0.04	0.15	0.17	0.28
70	32	457	BPSK	7	365	0.799	0.07	0.22	0.23	0.45
70	8	114	QPSK	7	182	1.598	0.13	0.22	0.24	0.48
70	16	228	QPSK	7	365	1.598	0.16	0.27	0.34	0.48
70	32	457	QPSK	7	730	1.598	0.22	0.33	0.36	0.48
90	8	88	BPSK	7	71	0.806	0.08	0.10	0.13	0.34
90	16	177	BPSK	7	143	0.806	0.10	0.16	0.17	0.31
90	32	355	BPSK	7	286	0.806	0.06	0.21	0.24	0.37
90	8	88	QPSK	7	143	1.612	0.13	0.23	0.43	0.49
90	16	177	QPSK	7	286	1.612	0.23	0.31	0.46	0.47
90	32	355	QPSK	7	573	1.612	0.16	0.31	0.47	0.48
40	8	200	BPSK	1, 3, 5, 7, 9, 11	155	0.775	-	-	-	-
40	16	400	BPSK	1, 3, 5, 7, 9, 11	310	0.775	-	-	-	-
40	32	800	BPSK	1, 3, 5, 7, 9, 11	620	0.775	-	-	-	-
40	8	200	QPSK	1, 3, 5, 7, 9, 11	310	1.550	-	-	-	-
40	16	400	QPSK	1, 3, 5, 7, 9, 11	620	1.550	-	-	-	-
40	32	800	QPSK	1, 3, 5, 7, 9, 11	1240	1.550	-	-	-	-

[a]The values of BER at several points of accumulated probability are given for the different values of OFDM length, number of carriers, and modulation. IBO, Input Back-Off; BW, Bandwidth.

4.1. DSSS Outcomes

The DSSS modem was evaluated using the BER over the received data for every PN sequence length and bandwidth (see Table 1). The DEVM is used to confirm the results already deduced from the BER. All BER and DEVM outcomes are computed using 148 blocks of 25 symbols for each experiment, as described in Figure 1.

4.1.1. Bit Error Rate

The results concerning BER for all combinations of bandwidth and PN sequence length can be found in Table 1. The results are shown by means of the cumulative distribution function (CDF) of four probabilities of BER: 10%, 30%, 50%, and 70%. The best configuration should expect a high probability value for a low BER. The best five combinations are the following: (i) Length 31 and BW = 250 Hz, (ii) Length 31 and BW = 500 Hz, (iii) Length 31 and BW = 1000 Hz, (iv) Length 63 and BW = 500 Hz, and (v) Length 63 and BW = 1000 Hz.

All the results concerning length 127 show worse performance than these four combinations. These results are corroborated with the average BER (in %) evaluated over all tests and shown in Figure 3 (left), as a function of the bit rate. The worst results in terms of average BER correspond to the widest bandwidths (20 kHz and 10 kHz)—related to high bit rates—and the longest possible symbol length (i.e., 400 samples per chip and 127 chips PN sequence). The best combinations (Figure 3 (right)) correspond to (i) Length 31 and

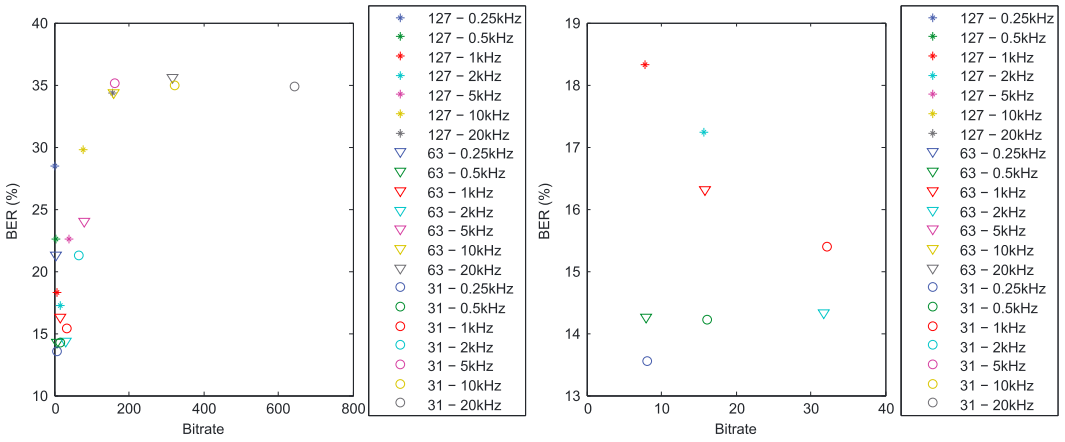

Figure 3. Average BER (in %) versus bit rate (in bps) for all the PN sequence lengths and bandwidth. (left) The whole results. (right) Only the combinations showing the best BER results.

BW = 250 Hz, (ii) Length 31 and BW = 500 Hz, (iii) Length 63 and BW = 500 Hz, and (iv) Length 63 and BW = 250 Hz together with Length 63 and BW = 2000 Hz.

The outcomes shown in Table 1 and Figure 3 agree on the best combinations of bandwidth and PN sequence length, which nearly have the lowest bit rate values. Moreover, Figure 3 shows that when increasing the bit rate, the BER worsens nearly exponentially. Therefore, in order to increase the throughput of the link, we think that a technique to increase the spectral efficiency [*Deumal et al.*, 2006] can be better than to decrease the symbol time.

In conclusion, the best results are achieved when combining a bandwidth of 250 Hz, 500 Hz, and 1000 Hz with sequences of 31 and 63 chips. If we carefully study Table 1 and Figure 3 we see that the longest symbol period does not give the lowest BER. As a clear example, PN sequence length 127 and bandwidths 250 Hz and 500 Hz show the worst results. This is due to the long symbol time length, which exceeds the coherence time of the channel (ranging from 500 ms to 1 s with Gaussian distribution of probability [*Ads et al.*, 2012]) and leads to demodulation errors at the receiver. We have to take into account that one symbol time T can reach 500 ms when transmitting sequences with 127 chips and 250 Hz of bandwidth, so high variations of the channel impulse response might occur while a single symbol is transmitted. Consequently, neither too short nor too long symbol length guarantee a good performance; hence, the best results are given by intermediate symbol lengths.

4.1.2. Differential Error Vector Magnitude

In order to compare the results of all possible combinations of bandwidth and PN sequence length, the measure given is not EVM but DEVM. The DEVM, although based on the performance analysis of EVM, is independent of the entire symbol energy due to the differential evaluation.

On the left side of Figure 4, we show the entire curve of CDF of DEVM of the nine best combinations obtained from BER analysis (see section 4.1.1). The best result is the curve that reaches the highest cumulative probability for a given value of DEVM. The best result is obtained with PN sequence length 31 and bandwidth 1000 Hz, followed by PN sequence length 31 and bandwidth 500 Hz, and the third best curve is PN sequence length 63 and bandwidth 500 Hz. So the results of CDF of the DEVM corroborate the results obtained by means of BER in Table 1, with minor variations.

4.2. OFDM Outcomes

The outcomes and conclusions related to OFDM tests are based on the reception of 33 blocks of 120 OFDM symbols for each experiment (i.e., symbol time length, number of subcarriers, constellation, and IBO), which are all summarized in Table 2.

4.2.1. Symbol Time Length

Concerning the symbol time length ($T_s = N_c T$), we tested five different values (see Table 2). On one hand, we expect that shorter symbols have a poorer performance than longer symbols due to the loss of SNR (see equation (5)) and also because the shorter the symbol length the wider the subcarrier separation and hence the worse the channel estimation. If we want to fulfill the Nyquist criterion in the frequency domain, when

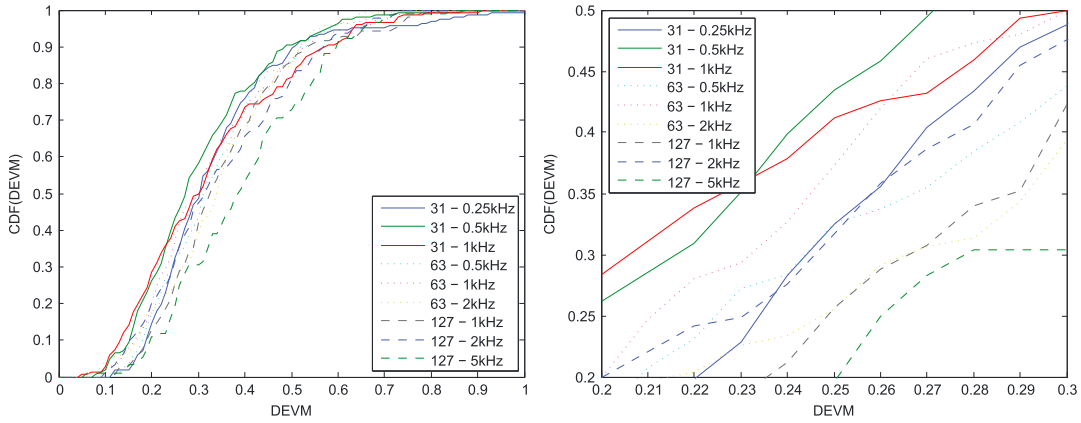

Figure 4. Cumulative distribution function of the DEVM, with the best combinations of the PN sequence lengths and bandwidth. (left) The whole results for the nine best combinations. (right) A detail of the evolution of the CDF(DEVM).

estimating the channel by means of OFDM pilot symbols (see section 3.2.1) at least two channel samples must be guaranteed inside the coherence bandwidth of the channel. We note that subcarrier separation in these tests ranges from 11 Hz to 100 Hz, which is inversely proportional to the symbol length $\left(T_s = \frac{1}{\Delta f}\right)$, while the coherence bandwidth of the channel ranges from 150 Hz to 500 Hz. Moreover, the longest symbol lengths (i.e., 90 *ms*) must fulfill the Nyquist criterion in the time domain and guarantee at least two samples inside the time coherence of the channel, which ranges from 500 *ms* to 1 *s*. As depicted in Figure 2 we estimate the channel every six symbols, and hence the sampling period of the channel ranges from 78 ms for the shortest symbols (10 ms) to 558 ms for the longest symbols (90 ms).

We present the outcomes of this section by means of the CDF of BER as well as by means of the root-mean-square of the EVM of the received symbols that can be defined as [*Forestier et al.*, 2004]

$$\mathrm{EVM}_{\mathrm{RMS}} = \sqrt{\frac{\frac{1}{N}\sum_{r=1}^{N} |S_{\mathrm{ideal},r} - S_{\mathrm{meas},r}|^2}{\frac{1}{N}\sum_{r=1}^{N} |S_{\mathrm{ideal},r}|^2}}, \tag{7}$$

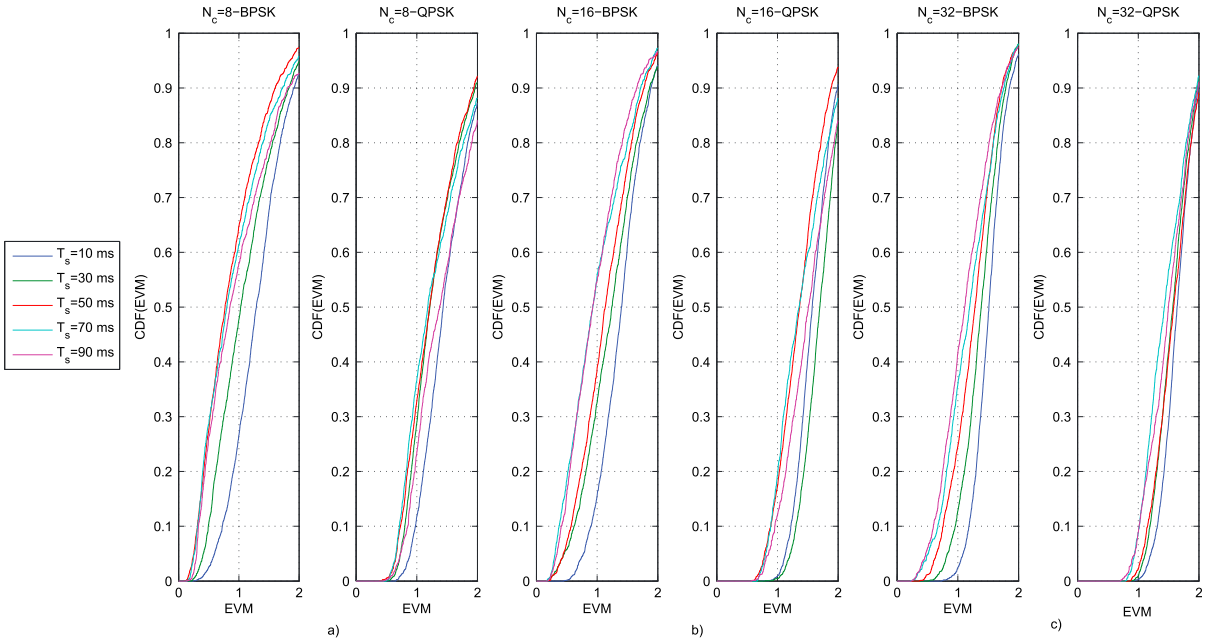

Figure 5. Cumulative distribution function of the EVM of all transmitted OFDM symbol lengths with (a) 8, (b) 16, and (c) 32 subcarriers modulated with BPSK (left) and QPSK (right).

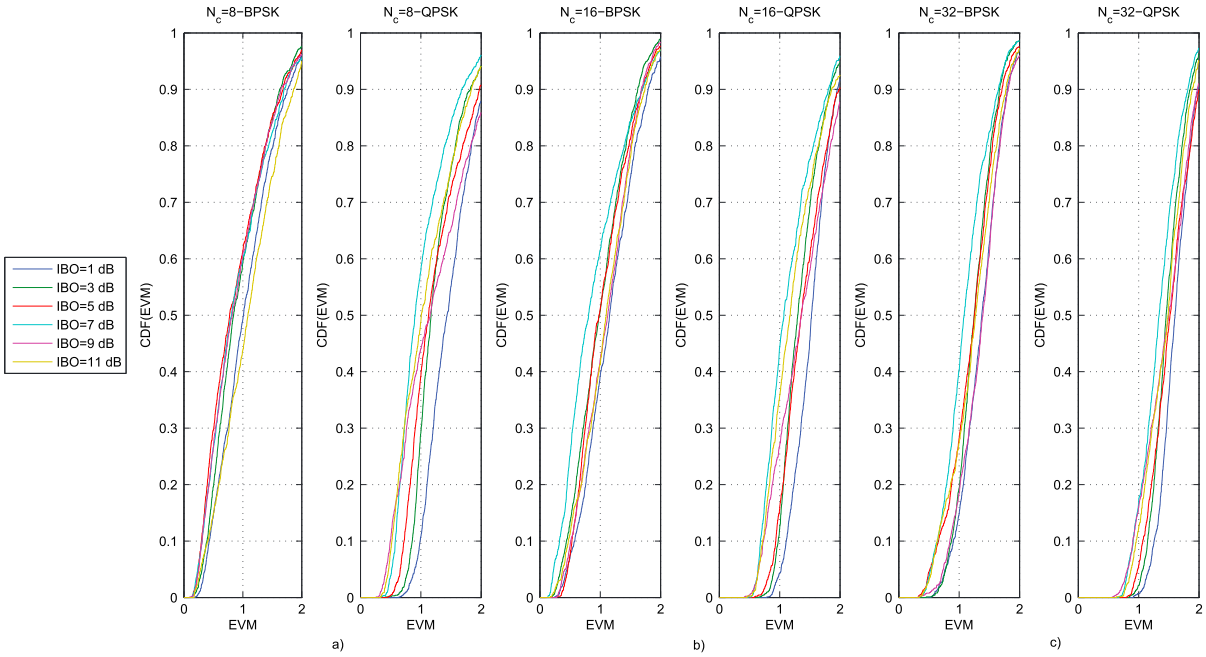

Figure 6. Cumulative distribution function of the EVM for different clipping levels applied to OFDM symbols with (a) 8, (b) 16, and (c) 32 subcarriers modulated with BPSK (left) and QPSK (right).

where $S_{ideal,r}$ is the ideal normalized point of the constellation for the r^{th} symbol, $S_{meas,r}$ is the normalized r^{th} symbol in the stream of measured symbols, and N is the number of unique symbols in the constellation, in our case $N = 2$ for BPSK and $N = 4$ for QPSK.

Figure 5 (divided into Figures 5a–5c) shows the results of CDF of the EVM for OFDM symbols with 8, 16, and 32 subcarriers, respectively. Each plot is divided in two halves, the left for the BPSK results and the right for the QPSK results. On each plot we depict the results of EVM of the 33×120 OFDM symbols that we received for each symbol length (i.e., 10, 30, 50, 70, and 90 ms). It is clear that in all plots, for each OFDM symbol length, BPSK always performs better than QPSK. The reason is that QPSK symbols are twice more efficient than BPSK symbols; and hence, QPSK requires a 3 dB higher SNR for the same $\frac{E_b}{N_0}$.

If we focus in BPSK figures, it is also clear that, given a symbol length, the higher the number of subcarriers the lower the power per subcarrier and hence the higher the EVM. We also remark the fact that shorter symbol lengths (i.e., 10 ms and 30 ms) always perform worse than longer ones due to the loss of SNR and the poor channel estimation explained in section 3.2.1. We note that the best symbol time length depends on the number of subcarriers and hence the bandwidth. For the case of 8 subcarriers, $T_s = 50$ ms obtains an EVM ≤ 1 in 64% of cases, whereas for 16 subcarriers, $T_s = 70$ ms gets the best performance with an EVM ≤ 1 in 56% of cases, and for 32 subcarriers, $T_s = 90$ ms gets the best performance with an EVM ≤ 1 in 41% of cases. This performance is due to the fact that those symbols that exceed the coherence bandwidth of the channel on average perform better than those that occupy a lower bandwidth which may completely coincide with a fading of the channel or a narrowband interference. A multicarrier system takes advantage of frequency diversity as long as it applies forward error correction codes and interleaving; however, in our case we already see a better performance of wider bandwidths when transmitting long symbol lengths without applying channel codification techniques.

In Table 2 we show the CDF of BER sampled at a probability of occurrence of 10%,30%,50%, and 70%. These values confirm the results obtained by means of the EVM: (i) BPSK always outperforms QPSK, (ii) the BER improves as the symbol length gets longer until 70 ms, and (iii) the longest symbol length (i.e., 90 ms) outperforms all other lengths only when the occupied bandwidth exceeds the coherence bandwidth of the channel, which happens at 32 subcarriers ($BW_{OFDM} = 355.5$ Hz).

Table 3. Summary of the Best Outcomes of DSSS and OFDM Receptions[a]

Symbol Characteristics	BW (Hz)	Symbol Time (ms)	BER ($P = 30\%$)	SNR ($P = 80\%$)(dB)	Bit Rate (bps)	Specific Efficiency (bps/Hz)
31 chips	500	62	0	−4.9	16.3	0.032
31 chips	250	124	0	−3.7	8.06	0.032
63 chips	1000	63	0.04	−5.5	15.87	0.016
63 chips	500	126	0	−5.8	7.94	0.016
50 × 8 BPSK	160	53	0.11	8.8	125	0.786
70 × 16 BPSK	228	73	0.15	7	91	0.799
90 × 32 BPSK	355	93	0.21	6	71	0.806

[a]The sequence length and the number of samples per chip are shown for DSSS, and for OFDM the symbol length, the number of subcarriers, and the constellation.

4.2.2. Input Back-off

In order to study the effect of clipping the envelope of the OFDM symbol to reduce the PAPR, we transmitted 33 × 120 OFDM symbols for each value of IBO (see Table 2). All symbols have the same length (i.e., 40 ms), 8, 16, and 32 subcarrier, and two types of constellations (BPSK and QPSK) were transmitted. We would like to remind the reader that high oversampling factors in the IFFT/fast Fourier transform are implemented due the low number of subcarriers and the long symbol periods (see section 3.2.1).

As in previous experiments, the CDF of the EVM and the BER are used to find the best performance. When analyzing the EVM by means of Figures 6a–6c, we highlight the fact that neither the lowest nor the highest value of IBO but a medium value (i.e., 7 dB) outperforms the others. This is because lowest values of IBO produce high in-band distortion that degrades the EVM whereas high values of IBO reduce the mean transmitted power, which is a critical issue. If we focus on BPSK outcomes, we note that as the number of subcarriers increases the majority of curves move from the one with IBO = 7 dB when $N_c = 8$ to the curve with IBO = 1 dB when $N_c = 32$. This may be due to the fact that the probability of getting high PAPR symbols increases with the number of subcarriers and also increases the probability to clip the symbol. Therefore, those values of IBO that do not produce high values of distortion with low number of subcarriers do increase in-band distortion with higher number of subcarriers.

5. Conclusions

In this paper we have analyzed a number of experiments on DSSS and OFDM data transmission over the HF channel between Antarctica and Spain. We gathered data from this ionospheric link during two Antarctic surveys to compare the performance of a low-efficiency technique, which is far below the capacity of the channel, with a high-efficiency technique, which transmits nearer the Shannon channel capacity upper bound [*Shannon*, 1948]. Table 3 summarizes the characteristics and performance of the best of both techniques.

The best DSSS results are obtained for time length between 62 ms and 126 ms (i.e., between 7.94 bps and 16.3 bps). Long DSSS symbols (i.e., 127 chips per symbol) always perform worse than short symbols (i.e., 31 chips per symbol) because long symbol lengths ($252\,\text{ms} \leq T \leq 508\,\text{ms}$) approximate the coherence time of the channel and hence experience high-phase rotation within a symbol time, which is impossible to be tracked. For a fixed a bit rate, the best BER performance is given by the symbol with narrowest bandwidth. Although symbols with wide bandwidth (i.e., 2 kHz) may benefit from frequency diversity, in this low SNR and highly interfered scenario, symbols with narrow bandwidth prevail. Therefore, it seems that this data link will not benefit from frequency diversity unless symbols with wide bandwidth are combined with long PN sequences (i.e 511, 1023, and 2047 chips per sequence) to minimize interfering signals due to the higher process gain [*Peterson et al.*, 1995].

The best OFDM results are obtained for symbol time lengths ranging between 50 and 90 ms (i.e., 71 and 125 bps). The achieved raw BER for these configurations shows that it is mandatory to implement channel coding and interleaving techniques to reduce the BER. Frequency diversity is only reached when the number of subcarriers is maximum (i.e., 32), although the power per subcarrier is minimum. Those symbols clipped at large IBO (i.e., 9 and 11 dB) and those clipped at low IBO (i.e., 1 and 3 dB) always perform worse than those clipped at medium values (5 and 7 dB). This performance may be due to the fact that the first

reaches the receiver with mean power below the noise floor, and the second leaves the transmitter with in-band distortion higher than the energy per symbol.

OFDM spectral efficiency is between 20 and 40 times higher than DSSS spectral efficiency, which enables a 10 to 15 times higher bit rate in the same bandwidth. However, for a given BER the DSSS SNR is 12 dB to 14 dB lower than the OFDM SNR. Therefore, DSSS is able to transmit symbols under extreme SNR conditions at a rate far below the channel capacity (i.e., 1000 bits/s with a bandwidth of 500 Hz at −4 dB SNR [*Shannon*, 1948]). Whereas OFDM is able to transmit symbols below the channel capacity with higher SNR (i.e., 650 bits/s with a bandwidth of 200 Hz at +7 dB SNR [*Shannon*, 1948]) using channel coding and interleaving techniques.

These two approaches enable to access the medium (HF channel) from two different ways. The first (DSSS) would permit transmitting long periods of time below the noise floor and therefore minimizing the interference to other users; whereas, the second (OFDM) would permit transmitting short and sporadic bursts of data, also minimizing the interference, with good channel conditions. As a result of this comparison we propose the following strategy: for the unidirectional Antarctic channel, when the forecast channel [*Vilella et al.*, 2008; *Ads et al.*, 2012] is poor use DSSS, but when the channel is good use OFDM combined with channel coding and interleaving.

Acknowledgment
This work has been funded by the Spanish Government under the projects CGL2006-12437-C02-01, CTM2008-03536-E, CTM2009-13843-C02-02, and CTM2010-21312-C03-03.

References

Ads, A., P. Bergadà, C. Vilella, J. Regué, J. Pijoan, R. Bardají, and J. Mauricio (2012), A comprehensive sounding of the ionospheric HF radio link from Antarctica to Spain, *Radio Sci.*, *48*, 1–12, doi:10.1029/2012RS005074.

Andersson, P. (1994), Performance of frequency-hopping radio systems on interference-limited HF channels, *6th International Conference on HF Radio Systems and Techniques,* York, U. K.

Baum, K., I. Schaumburg, and N. Nadgauda (1997), A comparision of differential and coherent reception for a coded OFDM system in a low C/I environment, *Global Telecommunications Conference*, vol. 1, pp. 300–304, Phoenix, Ariz.

Bergadà, P., M. Deumal, R. Alsina, and J. Pijoan (2009), Time interleaving study for an OFDM long-haul HF radio link, *11th International Conference on Ionospheric Radio Systems and Techniques,* Edinburgh, Scotland, U. K.

Bergadà, P., M. Deumal, C. Vilella, J. R. Regué, D. Altadill, and S. Marsal (2009), Remote sensing and skywave digital communication from Antarctica, *Sensors*, *9*(12), 10,136–10,157, doi:10.3390/s91210136.

Deumal, M., C. Vilella, J. Socoro, R. Alsina, and J. L. Pijoan (2006), A DS-SS signaling based system proposal for low SNR HF digital communications, *10th International Conference on Ionospheric Radio Systems and Techniques,* London, U. K.

D'Orazio, L., C. Sacchi, and F. D. Natale (2007), Multicarrier CDMA for data transmission over HF channels: Application to digital divide reduction, *IEEE Aerospace Conference,* Big Sky, Mont.

Engels, V., and H. Rohling (1995), Multilevel differential modulation techniques (64-dapsk) for Multicarrier Transmission System, *Eur. Trans. Telecommun.*, *6*, 633–640.

Forestier, S., P. Bouysse, R. Quere, A. Mallet, J.-M. Nebus, and L. Lapierre (2004), Joint optimization of the power-added efficiency and the error-vector measurement of 20-GHz pHEMT amplifier through a new dynamic bias-control method, *IEEE Trans. Microwave Theory Tech.*, *52*, 1132–1140.

Furman, W. N., and J. W. Nieto (2012), Latest on-air testing of U.S. MIL-STD-188-110C appendix D wideband HF data waveforms, *12th IET International Conference on Ionospheric Radio Systems and Techniques*, pp. 1–5, York, U. K.

Gherm, V., N. Zernov, and H. Strangeways (2005), HF propagation in a wideband ionospheric fluctuating reflection channel: Physically based software simulator of the channel, *Radio Sci.*, *40*, RS1001, doi:10.1029/2004RS003093.

Gold, R. (1968), Maximal recursive sequences with 3-valued recursive cross-correlation functions, *IEEE Trans. Inf. Theory*, *IT-14*, 154–156.

Gill, M. C., S. C. Cook, T. C. Giles, and J. T. Ball (1995), A 300 to 3600 bps multi-rate HF parallel tone modem, *Military Communications Conference*, vol. 3, pp. 1066–1070, San Diego, Calif.

Golomb, S. W. (1967), *Shift Register Sequences*, Holden-Day, San Francisco.

Hoeher, P., S. Kaiser, and P. Roberston (1997), Two-dimensional pilot-symbol aided channel estimation by Wiener filtering, *International Conference on Acoustics, Speech and Signal Processing,* Munich, Bavaria, Germany.

Johnson, E. E. (2009), Performance envelope of broadband HF data waveforms, *IEEE Military Communications Conference*, pp. 1–7, 18-21 Oct., Boston, Mass.

Moose, P. (1994), A technique for orthogonal frequency division multiplexing frequency offset correction, *IEEE Trans. Commun.*, *42*, 2908–2914.

Myung, H. G., and D. Goodman (2008), Single carrier FDMA: A new air interface for long term evolution, John Wiley, Hoboken, N. J.

NATO (1999), STANAG 4415, characteristics of a robust, non-hopping, serial-tone modulator/demodulator for severely degraded HF radio links, Edition 1, 21 June 1999.

Nieto, J. W. (2008), An investigation of coded OFDM and COFDM waveforms utilizing different modulation schemes on HF channels, *6th International Symposium on Communication Systems, Networks and Digital Signal Processing,* Reykjavik, Iceland.

Peled, A., and A. Ruiz (1980), Frequency domain data transmission using reduced computational complexity algorithms, *IEEE International Conference on Acoustics, Speech and Signal Processing*, pp. 964–967, Denver, Colo.

Perkiomaki, J. (2013), HF propagation prediction and ionospheric communications analysis. [Available at http//:www.voacap.com.]

Peterson, R. L., R. E. Ziemer, and D. E. Borth (1995), *Spread Spectrum Communications Handbook*, Prentice Hall, Upper Saddle River, N. J.

Proakis, J. (2000), *Digital Communications*, McGraw Hill, New York.

Sandell, M., J. van de Beek, and P. Börjesson (1995), Timming and frequency synchronization in OFDM systems using the cyclic prefix, *IEEE international Symposium on Synchronization,* Saalbau, Essen, Germany.

Schmidl, T., and C. Cox (1997), Robust frequency and timming synchronization for OFDM, *IEEE Trans. Commun.*, *45*, 1613–1621.

Shannon, C. E. (1948), A mathematical theory of communication, *The Bell Syst. Tech. J.*, *27*, 379–423.

Smith, O. J., M. J. Angling, P. S. Cannon, V. Jodalen, B. Jacobsen, and O. K. Gronnerud (2001), Simultaneous measurements of propagation characteristics on noncontiguous HF channels, *11th International Conference on Antennas and Propagation*, vol. 1, pp. 383-387, Manchester, U. K.

Tourtier, P., R. Monnier, and P. Lopez (1993), Multicarrier modem for digital HDTV terrestrial broadcasting, *Signal Process. Image Commun.*, *5*, 379–403.

US Department of Defense (1991), MIL-STD-188-110A, Military Standard: Interoperabilty and Performance Standards for Data Modems.

Vilella, C., D. Miralles, and J. Pijoan (2008), An Antarctica-to-Spain HF ionospheric radio link: Sounding results, *Radio Sci.*, *43*, RS4008, doi:10.1029/2007RS003812.

Vilella, C., D. Miralles, D. Altadill, F. Acosta, J. Sole, J. Torta, and J. Pijoan (2009), Vertical and oblique ionospheric soundings over a very long multihop HF radio link from polar to midlatitudes: Results and relationships, *Radio Sci.*, *44*, RS2014, doi:10.1029/2008RS004001.

Wagner, L. S., J. A. Goldstein, W. D. Meyers, and P. A. Bello (1989), The HF skywave channel: Measured scattering functions for midlatitude and auroral channels and estimates for short-term wideband HF rake modem performance, *IEEE Military Communications Conference*, vol. 3, pp. 830–839, Boston, Mass.

Zhang, H., H. Yang, R. Luo, and S. Xu (2005), Design considerations of a new HF modem and performance analysis, *IEEE International Symposium on Microwave, Antenna, Propagation and EMC Technologies for Wireless Communications,* Beijing, China.